

Potential High-Performance Magnet: Fe- and Zr-Alloyed Ce₂Co₁₇

Tribhuwan Pandey[✉] and David S. Parker*

Material Science and Technology Division Oak Ridge National Laboratory, Oak Ridge, Tennessee 37831, USA

(Received 31 July 2019; revised manuscript received 5 January 2020; accepted 18 February 2020; published 16 March 2020)

By performing comprehensive first-principles calculations, we study the hard magnetic properties of Ce₂Co₁₇ and Ce₂Fe₁₇ under Zr doping with varying Co concentrations, given the substantial experimental success of Zr in improving the magnetic anisotropy energy (MAE) in Ce₂Co₁₇ and Sm₂Co₁₇. We find that the magnetic properties of these alloys become comparable to state-of-the-art magnetic materials by doping with two elements, Zr and Fe, with potential-energy products BH_{\max} of 40 MG Oe. The Zr substitution is particularly helpful for improving the MAE, leading to a magnetic hardness parameter $K_1/\mu_0 M_s^2$ that significantly exceeds unity for a substantial range of Co concentrations (between 60% and 100% of the 3d-element concentration). The calculated MAE exhibits a strong dependence on the Co concentration, indicative of a likely valence fluctuation with Co alloying, and shows a maximum value of 7.78 MJ/m³ for 60% Co doping. Thus, upon experimental verification, these alloys may become competitors to the better-known permanent-magnet materials Nd₂Fe₁₄B and SmCo₅.

DOI: 10.1103/PhysRevApplied.13.034039

I. INTRODUCTION

Strong permanent magnets are indispensable for industrialized society, finding myriad applications in areas ranging from the automotive sector (for both electrified and petroleum-fueled vehicles) through power generation (such as wind-turbine generators) to computer hard disk drives and electric motors. The search for new and improved strong permanent magnets is therefore a substantial topic of worldwide research today, with numerous national and international efforts worldwide. Reducing the rare-earth content in the state-of-the-art permanent magnets (such as Nd₂Fe₁₄B) is of particular interest and is a commonly used strategy. The most notable examples involve reducing the Nd content in Nd₂Fe₁₄B by doping with La or Ce at the Nd site [1–4]. Another possible design scenario is *rehabilitation* of seemingly unpromising materials into high-performance magnets by elemental substitution, tuning of the composition, interstitial modifications, or other means. For example, recent experimental and theoretical studies [5,6] show that paramagnetic CeCo₃ can be transformed into a potential permanent magnet by Mg alloying. Ce is a rather abundant and therefore relatively inexpensive rare earth, so that Ce-based magnetic compounds are attractive for permanent magnet applications if sufficient magnetic anisotropy can be attained.

Ce forms many interesting magnetic compounds with the transition metals Fe and Co, such as CeCo₅, Ce₂Fe₁₇, and Ce₂Co₁₇. Among these, CeCo₅ has shown potential for possible applications due to its relatively high Curie

point (653 K) and large uniaxial magnetic anisotropy (9.5 MJ/m³) [7,8]. Ce₂Co₁₇, on the other hand, despite its very high Curie point (1023 K) and large saturation moment (1.1 T), remains a rather inferior magnet due to its rather small uniaxial magnetic anisotropy energy (MAE). It has previously been shown that the poor MAE of R₂Co₁₇ compounds stems from the negative contribution of the Co atoms occupying the “dumbbell” site in the rhombohedral structure [9]. Since then, many experimental studies have explored the possibility of improving the MAE of this material by substitutions at this dumbbell site by using Fe [10], Mn [10,11], Zr [10,12], Si [13], and Al [14,15]. Among these, the maximum MAE has been observed for Zr-doped Ce₂Co₁₇. By studying Sm₂Co₁₇, Larson *et al.* [16] showed that the MAE of 2-17 magnetic compounds can be significantly improved by Zr substitution for dumbbell-site Co atoms (one Zr → two Co). This huge increase in the MAE originates from a substantial lattice relaxation upon Zr alloying, which makes the Sm-Co distances comparable to the corresponding values in the very-high-MAE material ($K_1 = 17.2$ MJ/m³) SmCo₅. This concept has recently been extended to Ce₂Co₁₇ by Ke *et al.* [17], where they reported a factor-of-10 enhancement in the MAE by Zr substitution.

There is, however, a substantial downside of this substitution at the dumbbell site—a penalty to the magnetization. The highest magnetic moment for Co atoms in the Ce₂Co₁₇ rhombohedral structure is observed at the dumbbell site and the substitution of nonmagnetic Zr reduces the already relatively poor magnetic moment drastically. Therefore, for possible permanent magnet applications, the magnetic moment of Ce₂Co₁₅Zr needs to

* parkerds@ornl.gov

be improved. Here, by performing state-of-the-art first-principles density-functional-theory (DFT) calculations, we propose a possible solution of this problem in the $\text{Ce}_2\text{ZrFe}_{15-x}\text{Co}_x$ alloy. We begin with $\text{Ce}_2\text{Fe}_{17}$, a compound with an approximately 50% larger total magnetization than $\text{Ce}_2\text{Co}_{17}$, though it suffers from planar MAE (and is, in fact, a helimagnet rather than a ferromagnet), which does not change its sign even after Zr substitution at the dumbbell site. By substituting Co for Fe, we report that the MAE can be tuned to a very large uniaxial value of 7.78 MJ/m³ at 60%, Co alloying with relatively little sacrifice in terms of magnetic moment. Our assessment is that this enhancement in the MAE is related to Ce valence fluctuations in these compounds. From our electronic structure analysis, we conclude that for a Co concentration equal to or higher than 40%, Ce changes its valency from tetravalent to trivalent, leading to a transition from planar to uniaxial behavior and thereby a strong enhancement in the MAE.

II. METHODOLOGY

All first-principles calculations are performed within DFT using the general potential linearized augmented plane-wave (LAPW) method plus local orbitals [18,19] as implemented in the WIEN2K code [20]. The LAPW sphere radii are set to 2.30 Bohr for Ce and 1.83 Bohr for Fe, Co, and Zr. In addition, a RK_{\max} (the product of the smallest LAPW sphere radius (R) and the interstitial plane-wave cutoff, K_{\max}) of 9.0 is used to ensure a well-converged basis set. The calculations for $\text{Ce}_2\text{Fe}_{17}$ and $\text{Ce}_2\text{Co}_{17}$ are performed using the experimental lattice parameters with the internal coordinates relaxed. It is shown that upon Zr substitution at the dumbbell site (one Zr \rightarrow Co₂ or Fe₂), the volume of the unit changes by less than 2%. The calculations for $\text{Ce}_2\text{Fe}_{15}\text{Zr}$ and $\text{Ce}_2\text{Co}_{15}\text{Zr}$ are also performed at the experimental lattice parameters of the corresponding base compounds. The Co alloying at selected concentrations between $\text{Ce}_2\text{Fe}_{15}\text{Zr}$ and $\text{Ce}_2\text{Co}_{15}\text{Zr}$ is modeled within the virtual-crystal approximation (VCA). For the alloyed system $\text{Ce}_2\text{Fe}_{15-x}\text{Co}_x\text{Zr}$, the lattice parameters are modified according to Vegard's law [21,22]. For all the systems, the internal atomic coordinates are determined by minimizing the total energy using the generalized gradient approximation (GGA) of Perdew and coworkers [23] until the forces on all the atoms are less than 1 mRy/Bohr. For this purpose, 1000 reducible \mathbf{k} points are used in the full Brillouin zone. Although the VCA correctly predicts the magnetic moments, it can overestimate the MAE. To address this issue, the Co doping in $\text{Ce}_2\text{Fe}_{15}\text{Zr}$ is also studied, using the supercell method.

For the calculation of MAE, spin-orbital coupling (SOC) is included within the standard second-variational approach [24]. The MAE calculations are performed by using 5000 \mathbf{k} points. To check the convergence of the MAE

with respect to the number of \mathbf{k} points, additional calculations are performed with 4000 \mathbf{k} points. Upon this change, the MAE varies only by approximately 3%, demonstrating the excellent convergence of these calculations. All the calculations presented here correspond to 5000 \mathbf{k} points in the entire Brillouin zone. As is well known, the magnetic character of Ce (localized versus itinerant)—in particular, for Ce and transition-metal compounds—is debatable. Pressure chemical substitution can often induce itinerant-to-localized crossover [25,26]. The widely used extensions of DFT that can effectively describe electron localization are the self-interaction corrected–local spin-density (SIC-LSD) approximation [27] and the DFT + U methods [28]. In the SIC-LSD method [27,29,30], the total energy is corrected for spurious self-interaction of each localized state and this correction vanishes for an itinerant state. In the DFT + U method, a quadratic correction energy (which includes Hubbard repulsion and a double-counting term) is added to the Hamiltonian for better description of the correlated f electrons. For the localized case, in our calculations the rare-earth f orbitals are described within the DFT + U formalism, which adds a Hubbard U parameter and Hund's coupling parameter J to split the localized f orbitals above and below the Fermi level. The Coulomb correlations within the Ce-4f localized orbitals are described using the self-interaction correction scheme [31–33], which only depends on $U_{\text{eff}} = U - J$. Here, as in our previous work [3], a value of $U - J = 3$ eV for Ce is used. The density of states and magnetic properties from both GGA + SOC and GGA + SOC + U calculations are compared.

III. RESULTS AND DISCUSSION

A. Effect of Zr substitution on magnetic properties of $\text{Ce}_2\text{Fe}_{17}$ and $\text{Ce}_2\text{Co}_{17}$

We begin by calculating the magnetic properties of the base compounds $\text{Ce}_2\text{Fe}_{17}$ and $\text{Ce}_2\text{Co}_{17}$. Note that for the purposes of this work, we model $\text{Ce}_2\text{Fe}_{17}$ as a ferromagnet, despite the experimental presence [34–38] of helimagnetism: as we find the region of interest for permanent magnets to be generally on the Co-rich side of these compositions (where ferromagnetic behavior indeed prevails), this does not introduce appreciable error. To estimate the magnetic ground state for $\text{Ce}_2\text{Fe}_{15-x}\text{Co}_x\text{Zr}$ alloys at various Co concentrations, we carry out calculations of several collinear spin configurations, as shown in the Figure S1 in the Supplemental Material [39]. The energetics of these configurations are given in Table S1, which illustrates that the ferromagnetic configuration in which all Fe-Co atoms are aligned in the same directions is energetically the most favorable. This ferromagnetic behavior of $\text{Ce}_2\text{Fe}_{15-x}\text{Co}_x\text{Zr}$ alloys is supported by the previous experimental study of Shaheen *et al.* [40], which finds that

approximately 10% Co alloying in $\text{Ce}_2\text{Fe}_{17}$ yields a substantial room-temperature magnetization, or in other words a ferromagnet, as we have assumed. Additionally, the previous studies [10,12] on ferromagnetic $\text{Ce}_2\text{Co}_{17}$ find that under Zr alloying, this material remains ferromagnetic. These facts taken together strongly suggest that the ground state of our Fe- and Zr-alloyed $\text{Ce}_2\text{Co}_{17}$ material is in fact a ferromagnetic one.

The calculated magnetic moments and MAE values for $\text{Ce}_2\text{Fe}_{17}$ and $\text{Ce}_2\text{Co}_{17}$ are listed in Table I. For $\text{Ce}_2\text{Co}_{17}$, the calculated total (spin plus orbital) magnetization of $25.88 \mu_B$ per formula unit is in very good agreement with the measured value of $26.6 \mu_B$ [10,12]. Similar to numerous other rare-earth magnets [3,6,41], the Ce spin magnetic moment prefers to be antialigned with respect to Co, with average spin moments of $-0.66 \mu_B$ and $-0.96 \mu_B$ for the Fe and Co end-member compounds, respectively. In accordance with Hund's third rule, the Ce orbital moment is antiparallel to the spin moment. For $\text{Ce}_2\text{Co}_{17}$, our calculations find a small uniaxial MAE of approximately 0.4 MJ/m^3 from DFT + U calculations, which is in excellent agreement with the 5 K measured experimental value of 0.55 MJ/m^3 [10,12]. By omitting the Hubbard U from our calculations, a MAE value of 0.44 MJ/m^3 is obtained, which is comparable with the MAE obtained from DFT + U calculations with $U_{\text{Ce}} = 3 \text{ eV}$.

This MAE value is substantially lower than the approximately 4.5 MJ/m^3 MAE for the state-of-the-art permanent magnet $\text{Nd}_2\text{Fe}_{14}\text{B}$ and it renders this material unsuitable as a hard permanent magnet. The most promising way to enhance the MAE of 2-17 magnets has been proposed by Larson *et al.* [16] in $\text{Sm}_2\text{Co}_{17}$. They have suggested that the MAE of $\text{Sm}_2\text{Co}_{17}$ may become comparable to that of

SmCo_5 by a single Zr substitution for two Co “dumbbell”-site atoms. Such a substitution is sensible considering the more than twice as large atomic volume of Zr relative to Co. This has later been confirmed in $\text{Ce}_2\text{Co}_{17}$, by Ke *et al.* [17], where by Zr doping at the dumbbell site, they have reported a significant enhancement in the MAE. Here, for completeness, we recalculate the magnetic properties of $\text{Ce}_2\text{Fe}_{17}$ and $\text{Ce}_2\text{Co}_{17}$ under Zr substitution, which are described in Table I.

First, we discuss the effect of Zr substitution on the structural and magnetic properties of $\text{Ce}_2\text{Fe}_{17}$ and $\text{Ce}_2\text{Co}_{17}$. The nearest-neighbor (NN) distances between Ce and various M (Co-Fe) Wyckoff sites with and without Zr substitution are shown via a heat map in Fig. 1(c). In the base structure Ce_2M_{17} ($\text{Ce}_2\text{Fe}_{17}$ or $\text{Ce}_2\text{Co}_{17}$), the NN distances between Ce_{6c} and the M_{18f} , M_{18h} , and M_{6c} sites are comparable, followed by the $\text{Ce}_{6c}\text{-M}_{9d}$ distance. Upon Zr substitution at the Ce_2M_{17} ($M = \text{Fe}, \text{Co}$) dumbbell site shown by the red shaded ellipse in Fig. 1(a), the distance between the Ce_{6c} and M_{18f} sites is significantly decreased. A reduction can also be seen in the distance between the Ce_{6c} and M_{9d} sites, whereas the distance between the $\text{Ce}_{6c}\text{-M}_{18h}$ and $\text{Ce}_{6c}\text{-Ce}_{6c}$ sites increases. In particular, these Ce-NN distances are comparable to those in CeFe_5 (first NN, 2.806 \AA ; second NN, 3.147 \AA) and CeCo_5 (first NN, 2.845 \AA ; second NN, 3.179 \AA). This is consistent with the structure-relaxation effects reported in $\text{Sm}_2\text{Co}_{17}$ under Zr doping [16]. We observe that on $\text{Co}_2 \rightarrow \text{Zr}$ substitution, the spin magnetic moment of the Co_{9d} site increases by $0.46 \mu_B$ to $1.54 \mu_B$ and the moment on the Co_{18f} site decreases by $0.19 \mu_B$. As expected, due to substitution of a nonmagnetic element, the total magnetic moment for $\text{Ce}_2\text{Co}_{15}\text{Zr}$ reduces to $21.14 \mu_B$ per formula unit.

TABLE I. The calculated spin magnetic moments at various atomic sites, the total (spin plus orbital) magnetic moment, and the magnetic anisotropy calculated within the GGA by including spin-orbital coupling with a Hubbard U parameter of 3 eV at the Ce site. The calculations for $\text{Ce}_2\text{Fe}_{17}$ and $\text{Ce}_2\text{Co}_{17}$ (and the corresponding Zr-doped compounds) are performed using the experimental lattice parameters adopted from Refs. [37] and [10], respectively. The calculated formation energies (E^{for}) with respect to elemental decomposition are also shown. The E^{for} is calculated without spin-orbital coupling and without U . For the alloyed systems, the lattice parameters are scaled according to Vegard's law. All the lattice parameters employed in our work are listed in the table. Here, the Co doping is performed within the VCA.

Parameter	Compounds							
	$\text{Ce}_2\text{Fe}_{17}$	$\text{Ce}_2\text{Fe}_{15}\text{Zr}$	$\text{Ce}_2\text{Fe}_{12}\text{Co}_3\text{Zr}$	$\text{Ce}_2\text{Fe}_9\text{Co}_6\text{Zr}$	$\text{Ce}_2\text{Fe}_6\text{Co}_9\text{Zr}$	$\text{Ce}_2\text{Fe}_3\text{Co}_{15}\text{Zr}$	$\text{Ce}_2\text{Co}_{15}\text{Zr}$	$\text{Ce}_2\text{Co}_{17}$
$a (\text{\AA})$	8.489	8.489	8.468	8.447	8.425	8.404	8.383	8.383
$c (\text{\AA})$	12.408	12.408	12.371	12.334	12.297	12.260	12.223	12.223
$\mu_{\text{Ce-(6c)}} (\mu_B)$	-0.66	-0.48	-0.52	-0.92	-0.90	-0.85	-0.80	-0.96
$\mu_{\text{Zr}} (\mu_B)$	-0.27	-0.28	-0.28	-0.28	-0.27	-0.24		
$\mu_{\text{Fe/Co-(6c)}} (\mu_B)$	2.56							1.70
$\mu_{\text{Fe/Co-(9d)}} (\mu_B)$	2.05	2.04	2.17	2.05	1.91	1.73	1.54	1.08
$\mu_{\text{Fe/Co-(18f)}} (\mu_B)$	2.36	2.20	2.14	2.02	1.85	1.64	1.41	1.60
$\mu_{\text{Fe/Co-(18h)}} (\mu_B)$	2.22	2.13	2.20	2.10	1.94	1.75	1.54	1.56
$M_{\text{TOT}} (\mu_B \text{ per unit cell})$	38.04	30.26	30.77	28.92	27.15	24.12	21.14	25.88
$K_1 (\text{MJ/m}^3)$	-1.97	-5.54	-5.36	2.23	7.78	5.17	4.67	0.40
E^{for} (meV/atom)	-44.0	-80.0	-88.0	-110.0	-114.0	-112.0		

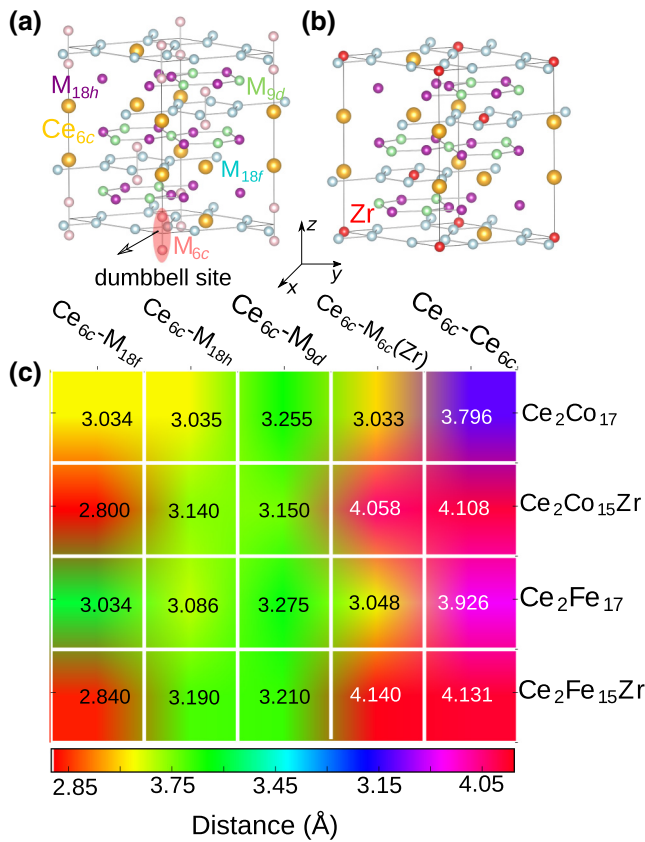


FIG. 1. (a) The rhombohedral crystal structure of the Ce_2M_{17} ($\text{M} = \text{Co}$ or Fe) unit cell, with all the crystallographic Wyckoff sites denoted by corresponding atomic site colors. (b) The crystal structure of $\text{Ce}_2\text{M}_{15}\text{Zr}$ after substituting one Zr atom (shown in red) for two dumbbell-site M atoms [the $\text{Fe}(\text{Co})-6c$ site is shown by the shaded area in (a)]. (c) The nearest-neighbor (NN) Ce-M and Ce-Zr distances in Ce_2M_{17} and $\text{Ce}_2\text{M}_{15}\text{Zr}$. Here, M refers to either Fe or Co. For comparison, the first two Ce NN distances in CeFe_5 and CeCo_5 are 2.806 Å, 3.147 Å and 2.845 Å, 3.179 Å, respectively.

In agreement with previous studies, we find that for $\text{Ce}_2\text{Co}_{15}\text{Zr}$, the MAE increases to 4.67 MJ/m³, which is ten times higher than the corresponding value for $\text{Ce}_2\text{Co}_{17}$. By analyzing the contribution from crystallographic sites, Ke *et al.* [17] have proposed that Zr substitution at the dumbbell site eliminates the negative contribution from the Co dumbbell sites, which results in a huge MAE. Previously, many experimental studies have investigated the effects of various transition-metal-atom dopings such as Zr, Hf, Ti, V, Cr, Mn, Fe, and Cu on the Co site [10–15]. Among these, the highest enhancement in anisotropy field has been found for Zr doping at the Co site [10,12]. By performing structural analysis, Wallace and coworkers [10,12] have shown that upon Zr substitution, the volume (per formula unit) of $\text{Ce}_2\text{Co}_{17}$ increases slightly, from 247.5 Å³ to 249.4 Å³. Since the atomic radius of Zr is larger than that of Co and smaller than that of Ce, this

volume enhancement suggests that Zr prefers to substitute for Co atoms. Note that this volume increase is driven by the increase in the in-plane lattice parameter a and a small decrease in the out-of-plane lattice parameter c , which implies that Zr substitution at the dumbbell site is preferred. This claim can be further validated by comparing the measured and calculated magnetic properties. The experimental measurements [10,12] for a sample of stated composition $\text{Ce}_2\text{Co}_{16}\text{Zr}$ show a MAE of 3.13 MJ/m³ and a saturation magnetization of 20 μ_B per formula unit at 77 K. These values are captured in our calculations ($M_s = 21.72 \mu_B$ per formula unit and MAE = 4.67 MJ/m³) where one Zr atom replaces a Co_2 dumbbell ($\text{Zr} \rightarrow \text{Co}_2$). Note that the MAE calculated [17] by replacing both Co_2 -dumbbell atoms by Zr atoms is only 0.95 MJ/m³. This is much smaller than the measured experimental value and strongly suggests that Zr most likely substitutes for two Co at the dumbbell site, as we and previous authors assume.

B. Magnetic properties of $\text{Ce}_2\text{ZrFe}_{15-x}\text{Co}_x$ alloys

As described above, although the MAE of $\text{Ce}_2\text{Co}_{17}$ can be improved by Zr substitution, it significantly reduces the magnetization. Next, we investigate the possibility of improving the magnetic properties of $\text{Ce}_2\text{Fe}_{15}\text{Zr}-\text{Ce}_2\text{Co}_{15}\text{Zr}$ by Co-Fe alloying. The magnetic properties as a function of various composition ranges between $\text{Ce}_2\text{Fe}_{15}\text{Zr}$ and $\text{Ce}_2\text{Co}_{15}\text{Zr}$ are studied within the VCA. Within the VCA, the random-atom occupation between two types of atoms are treated by using an averaged-charge virtual atom. In order to model the alloyed compound, the lattice parameters within the composition range, which are listed in Table I, are scaled according to Vegard's law [22]. Using these lattice parameters at each alloy composition, the atomic positions are optimized until the forces are less than 1 mRy/Bohr. The computed magnetic properties at various Co concentrations are listed in Table I. The total magnetization and the MAE as a function of the Co doping (x) are plotted in Figs. 2(a) and 2(b), respectively. Here, results of calculations both without U and with $U_{\text{Ce}} = 3$ eV are shown. As shown in Fig. 2(a), while with Co doping, in general the total magnetic moment of the system decreases, it still maintains a significant value of 27.15 μ_B per formula unit for $\text{Ce}_2\text{Fe}_6\text{Co}_9\text{Zr}$ alloy. This value of the total magnetic moment is only 1.1 times smaller than that of the end-member compound $\text{Ce}_2\text{Fe}_{15}\text{Zr}$, and 1.3 times higher than the magnetic moment of $\text{Ce}_2\text{Co}_{15}\text{Zr}$. We find that for $\text{Ce}_2\text{ZrFe}_{15-x}\text{Co}_x$, when the Co doping is less than 40% ($x < 6$), the MAE remains planar and as the Co substitution exceeds 40% ($x > 6$), the MAE switches to uniaxial. The highest uniaxial anisotropy, with MAE = 7.78 MJ/m³, occurs for 60% Co doping in $\text{Ce}_2\text{Fe}_6\text{Co}_6\text{Zr}$ alloy. This MAE is 1.6 times larger than that of $\text{Ce}_2\text{Co}_{15}\text{Zr}$. These calculated properties show that

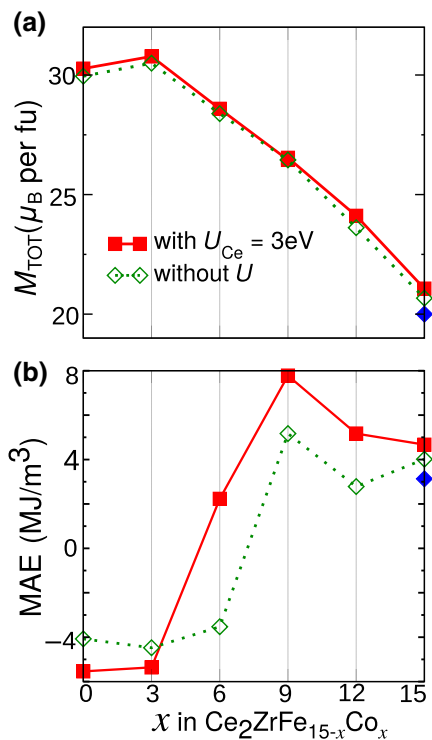


FIG. 2. (a) The total magnetic (spin plus orbital) moment and (b) the MAE in $\text{Ce}_2\text{ZrFe}_{15-x}\text{Co}_x$ as a function of x . Here, the Co doping is performed within the VCA. The symbols correspond to the calculated compositions and the line is a guide to the eye. The blue diamonds represent experimental data from Refs. [10,12]. Results from calculations both without the Hubbard U (open green diamonds) and with the Hubbard $U_{\text{Ce}} = 3 \text{ eV}$ (red filled squares) are compared here.

$\text{Ce}_2\text{ZrFe}_{15-x}\text{Co}_x$ alloys may exhibit performance comparable to the state-of-the-art permanent magnets. As shown in Fig. 2(b), enhancement of the MAE has also been observed in calculations without the Hubbard U parameter. Although the MAE is relatively smaller compared to the Hubbard U_{Ce} calculation, it is still sufficiently large (at 5.16 MJ/m^3 for the 60%-Co case) for a strong permanent magnet, given the magnetic hardness parameter $\kappa = K_1/\mu_0 M_s^2$ of 4.05 even at this lesser MAE value. Additionally, along with Ce f electrons, we also explore the effect of localization on Co d electrons. For this purpose, GGA + U calculations are performed for the Co end-member compounds ($\text{Ce}_2\text{ZrCo}_{15}$) and the 60% Co-doped case ($\text{Ce}_2\text{ZrFe}_6\text{Co}_9$), using a U of 3 eV only on Co site, and on both Co and Ce sites. However, as described in Table S2 of the Supplemental Material [39], this yields unphysically large MAE values exceeding 30 MJ/m^3 for the experimentally known end-member case (experimental measurements [10,12] for $\text{Ce}_2\text{Co}_{16}\text{Zr}$ show a MAE of 3.13 MJ/m^3 at 77 K). Therefore, we consider that any effects of Co localization are not sufficient to warrant applying the GGA + U approach to the Co atom itself. It is noteworthy

that while the MAE values calculated with and without the Hubbard U are slightly different (particularly at 60% Co doping), they follow the same qualitative trend. Besides, our previous studies on Ce-Co compounds— $\text{Ce}_2\text{Co}_9\text{Mg}$ [5,6], and CeCo_5 [8]—show that localized treatment of Ce f electrons is important in order to obtain the correct MAE. For example, the MAE for $\text{Ce}_2\text{Co}_9\text{Mg}$ calculated without the Hubbard U is only 0.46 MJ/m^3 smaller than the experimental MAE value of 2.2 MJ/m^3 . By including $U_{\text{Ce}} = 1.5 \text{ eV}$, a MAE of 2.10 MJ/m^3 is obtained, which is in excellent agreement with the experimental data. Similarly, for CeCo_5 , the MAE calculated without the Hubbard U is 3.17 MJ/m^3 , which is smaller than the experimental value of 10.5 MJ/m^3 . However, a DFT + U calculation with $U_{\text{Ce}} = 3.0 \text{ eV}$ gives a MAE of approximately 9.0 MJ/m^3 , which is in good agreement with the experimental value. These results suggest the likelihood of substantial localization of Ce f electrons in Ce-Co compounds.

Next, in order to understand this enhancement in the MAE, we analyze the density of states (DOS) at various Co concentrations in $\text{Ce}_2\text{ZrFe}_{15-x}\text{Co}_x$, which are shown in Figs. 3(a)–3(e). The DOS near the Fermi level predominantly originates from Ce f and Fe-Co d states. As shown in Fig. 3, the Ce f states (black and orange filled lines) are partially occupied in the spin-down channel and empty in the spin-up channel, confirming that the Ce spin moment antialigns with Fe-Co spin moments. The enhanced ($\times 15$) Zr DOS (red dashed line) is also shown for comparison. Although the Zr DOS at the Fermi level is relatively small, there is some hybridization present with the neighboring Ce and Co atoms. The magnetic properties of Ce-transition-metal compounds have been shown to be sensitive to the valence of Ce [11,42–45]. However, the accurate Ce f valence in Ce-transitional metal compounds is still debatable, previous studies having reported the occurrence of mixed Ce valency [44–48]. In particular, for $\text{Ce}_2\text{Fe}_{17}$ and $\text{Ce}_2\text{Co}_{17}$, x-ray absorption spectroscopy analysis suggests a Ce valence between 3.0 and 3.3 [44,45].

Perhaps the most intriguing feature of the DOS is the modification of the Ce valence by the varying Co concentration, which is clearly demonstrated in Fig. 4(a). The DOS for three representative cases ($\text{Ce}_2\text{Co}_{15}\text{Zr}$, $\text{Ce}_2\text{ZrFe}_6\text{Co}_{15}$, and $\text{Ce}_2\text{Co}_{15}\text{Zr}$) with $U_{\text{Ce}} = 3 \text{ eV}$ and without U is compared in Fig. S2 of the Supplemental Material [39]. For $\text{Ce}_2\text{ZrFe}_{15-x}\text{Co}_x$, when the Co doping is less than 40% ($x < 6$), the main localized Ce f states are situated above the Fermi level, with the band tail extending below the Fermi level. This indicates tetravalency of Ce in these particular alloys. As the Co doping exceeds 40% ($x > 6$), some of these localized Ce f states shift below the Fermi level, which should correspond to trivalent Ce. While the occupied $4f$ peak appearing for 40% and greater Co concentrations is relatively small, its presence is sufficient to yield large increases in the magnitudes

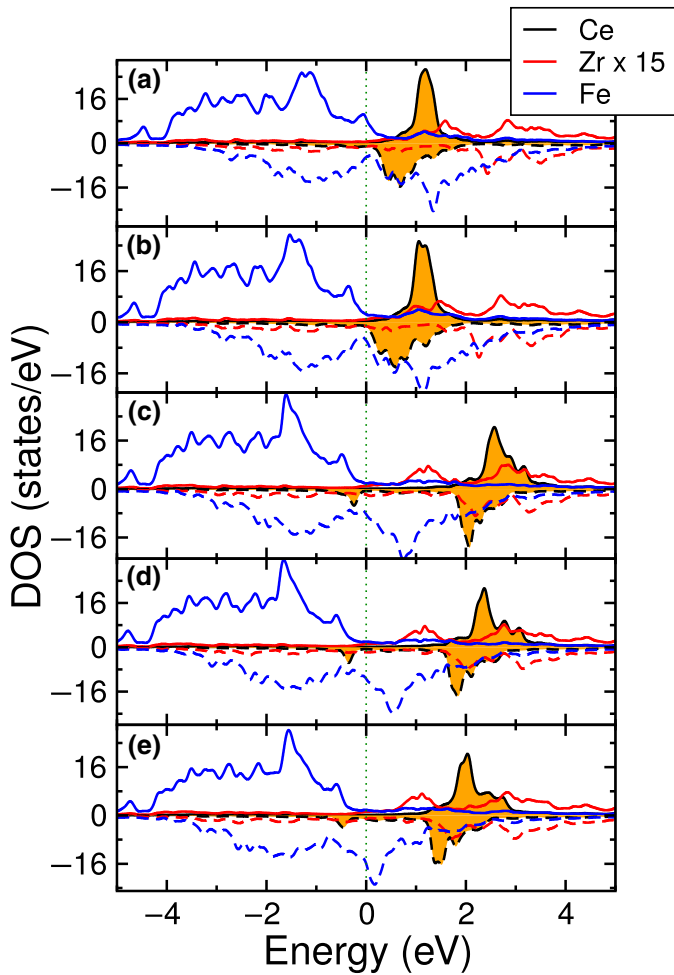


FIG. 3. The Ce f (black and orange filled lines) and Co plus Fe d , density of states (DOS) (blue lines) and the Zr DOS (red lines) in (a) $\text{Ce}_2\text{Fe}_{15}\text{Zr}$, (b) $\text{Ce}_2\text{Fe}_{12}\text{Co}_3\text{Zr}$, (c) $\text{Ce}_2\text{Fe}_9\text{Co}_6\text{Zr}$, (d) $\text{Ce}_2\text{Fe}_6\text{Co}_9\text{Zr}$, and (e) $\text{Ce}_2\text{Co}_{15}\text{Zr}$, calculated within GGA + SOC + U . The Zr DOS is enlarged by a factor of 15 for clarity. The Co-Fe DOS is averaged over all Co and Fe atoms. The spin-up and spin-down states are shown by the positive and negative values, respectively.

of both the Ce spin and orbital moments [see Fig. 4(b)], which ultimately yield the large MAE. This switching of the Ce valency on Co concentration can be correlated with calculated Ce spin (M_{SPIN}) and orbital magnetic moments (M_{ORB}), which are shown on the left- and right-hand y axes in Fig. 4(b). As the Ce valency switches from tetravalent (Ce^{4+}) to trivalent (Ce^{3+}), both the spin and the orbital magnetic moments exhibit significant increases. For example, in $\text{Ce}_2\text{Zr}\text{Fe}_{15}$ (where Ce is in the tetravalent state), the spin and orbital moments are $-0.48 \mu_B$ and $0.18 \mu_B$, respectively. For 40% Co doping, the Ce spin and orbital moments increase (in magnitude) to $-0.92 \mu_B$ and $0.57 \mu_B$. This behavior is consistent with the fact that Ce^{3+} is more magnetic than Ce^{4+} . Although the reason for the appearance of this $4f$ peak remains unclear, previous

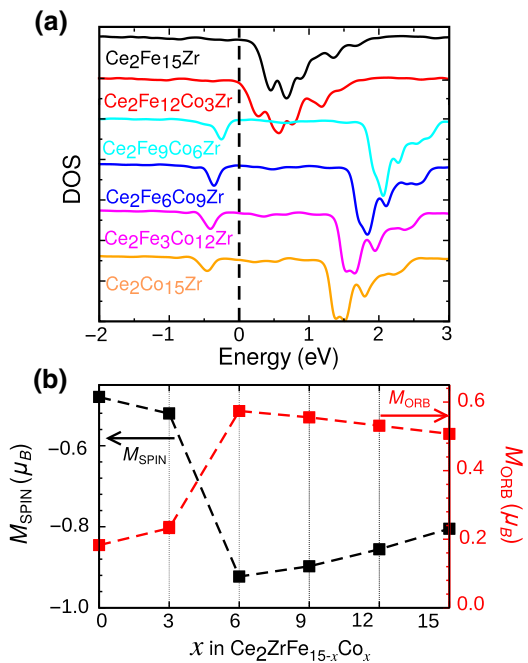


FIG. 4. (a) The modification in Ce spin-down f DOS on going from $\text{Ce}_2\text{Fe}_{15}\text{Zr}$ to $\text{Ce}_2\text{Co}_{15}\text{Zr}$ at various Co concentrations, calculated under GGA + SOC + U . For 40% Co concentration ($\text{Ce}_2\text{Fe}_9\text{Co}_6\text{Zr}$) and onward, the valency of Ce switches from tetravalent to trivalent. For clarity, the DOS plots have been shifted vertically with respect to one another. The Ce valency transition is also reflected in the Ce spin (M_{SPIN} , marked on the left-hand y axis) and orbital (M_{ORB} , marked on the right-hand y axis) moments shown in (b), where an abrupt increase is observed for 40% Co concentration.

reports [25,26] have shown that the itinerant or localized nature of Ce can be sensitive to the volume, the surrounding local environment, and chemical substitution. This suggests that the $4f$ peak for $\text{Ce}_2\text{Zr}\text{Fe}_{15-x}\text{Co}_x$ alloys can be attributed to volumetric or chemical-pressure effects associated with the 4% smaller volume of the end-member Co compound, relative to the Fe end member, as shown in Table I. Although we do not confirm the possibility of valence fluctuation, the sharp increase in the MAE along with the magnetic moments supports our hypothesis of Ce-valence fluctuation as a function of the Co concentration in these alloys.

To explain the calculated enhancement of the magnetic properties, we next analyze the anisotropy of the orbital magnetic moment. The Ce and Fe-Co orbital magnetic moments along the in-plane (a -axis) and out-of-plane (c -axis) directions are plotted in Figs. 5(a) and 5(b), respectively. The Co-Fe orbital magnetic moments are averaged over all the sites. The anisotropy of orbital moments (ΔM_{ORB}) is computed by taking the difference between the orbital magnetic moments along the c and a directions. Both the Ce and Fe-Co sites exhibit substantial orbital magnetic moment anisotropy, which increases with

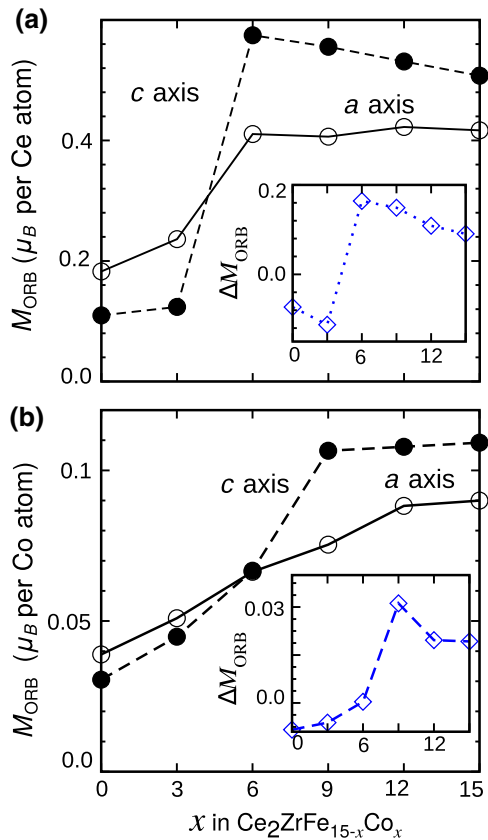


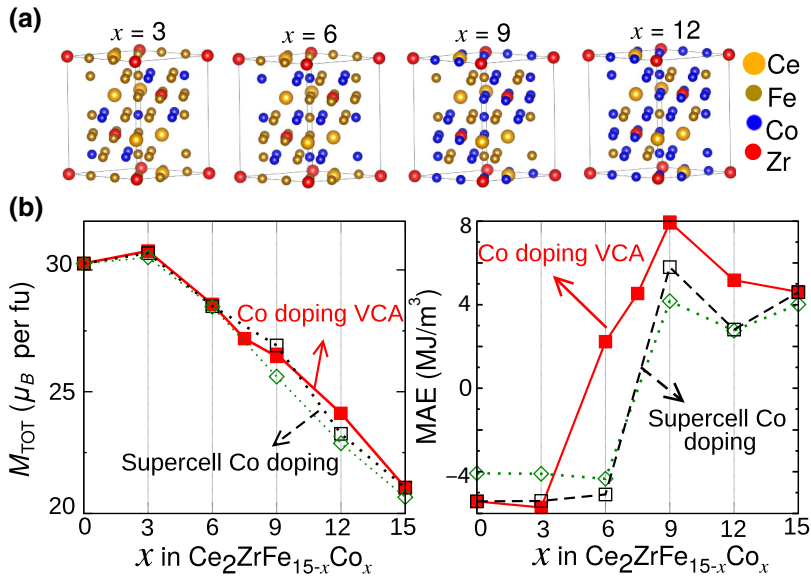
FIG. 5. (a) The orbital magnetic moment M_{ORB} (a) for Ce sites and (b) for Co-Fe sites as a function of x in $\text{Ce}_2\text{ZrFe}_{15-x}\text{Co}_x$, calculated under GGA + SOC + U . The insets give the anisotropy of the orbital magnetic moment ($\Delta M_{\text{ORB}} = M^c - M^a$).

Co concentration. With increasing Co doping, the relatively small value of $M_{\text{ORB}}^{\text{Ce}} = -0.07$ ($M_{\text{ORB}}^{\text{Fe}} = -0.008$) in $\text{Ce}_2\text{ZrFe}_{15}$ increases to 0.142 (0.03) for 60% Co doping (in $\text{Ce}_2\text{Fe}_6\text{Co}_9\text{Zr}$). Both $M_{\text{ORB}}^{\text{Ce}}$ and $M_{\text{ORB}}^{\text{Fe}}$ exhibit a nonmonotonic dependence on the Co concentration and exhibit maxima at 40% and 60% doping, respectively. According to Bruno's theorem [49], the MAE is directly proportional to the anisotropy of the orbital magnetic moment and can be described as $\text{MAE} = \sum_i \Delta M_{\text{ORB}}^i \Lambda_{\text{SOC}}^i S_i$. Here, Λ_{SOC}^i , ΔM_{ORB}^i , and S_i refer to the spin-orbital coupling constant, the anisotropy of the orbital moments, and the spin moment of atomic site i . As suggested by Bruno's formula, the MAE [Fig. 2(b)] and the anisotropy of the orbital moments exhibit (Fig. 5) nearly the same dependence on the Co concentration. If the interaction between Ce and transition-metal sublattice can be ignored, the MAE can be linearly expanded in terms of Ce and transition-metal sublattice. Given that the strength of the SOC for $4f$ rare-earth elements is an order of magnitude larger than that for Fe-Co, it indicates that a sizable fraction of the MAE will originate from Ce sites. At the same time, the substantial $M_{\text{ORB}}^{\text{Fe}/\text{Co}}$ suggests that Fe-Co will also make some valuable

contribution to the MAE. This is in accord with the substantial uniaxial MAE of CaCu_5 -structure materials such as LaCo_5 and YCo_5 , which entirely lack the $4f$ electrons that are usually believed to create large MAE [50].

The magnetic properties calculated above show the substantial potential for application as permanent magnets. However, as shown in previous studies, the VCA can overestimate the MAE [51,52]. Therefore, to confirm the improved MAE under Co alloying, calculations are also performed by modeling Co doping within a supercell approach [52,53]. The Fe atoms are replaced by Co atoms to form the various $\text{Ce}_2\text{ZrFe}_{15-x}\text{Co}_x$ -type alloy compositions. In total, four alloy compositions are studied by replacing three, six, nine, and 12 Fe atoms by Co. Due to the large number of nonequivalent atomic sites, the utilization of a supercell-based method for the MAE calculation is a computationally expensive task. Hence, we study only the cells in which rhombohedral symmetry is preserved. For this purpose, the sites for Co doping are selected such that the crystallographic site symmetry is preserved. This procedure results in one, two, two, and one configuration for 20, 40, 60, and 80% Co doping, respectively. After Co substitution, the atomic positions in all the structures are relaxed until the forces are less than 1 mRy/Bohr. Subsequently, the lowest-energy structure (for the 40% and 60% Co doping cases) is used for the magnetic property calculations, which are shown in Fig. 6(a). For the 60% Co case, which we identify as the optimal alloy, this structure is some 100 meV lower than the other considered structures, so that this structure is significantly favored energetically. The total magnetic moments and MAE for $\text{Ce}_2\text{ZrFe}_{15-x}$ as a function of x , calculated within the supercell approach, are shown in Figs. 6(b) and 6(c), respectively. Here, the results obtained within the VCA method are also shown for comparison. As expected, both the supercell method and the VCA method produce nearly the same magnetic moments. The situation is, however, somewhat different for the MAE, where we see that the MAE switches from planar to uniaxial at 60% Co doping, as opposed to 40% as observed with the VCA method. Within the supercell method at 60% Co doping, the calculated MAE is approximately 5.8 MJ/m^3 , slightly smaller than the VCA value of 7.78 MJ/m^3 . Nonetheless, for 60% and higher Co concentrations, the calculated MAE within the supercell method and the VCA method are in reasonable agreement. The total magnetization and MAE calculated with no U are also shown in Figs. 6(a) and 6(b) by green dotted lines with open diamonds. Similar to the VCA case, while the calculated MAE with no U is relatively smaller than $U_{\text{Ce}} = 3 \text{ eV}$, it is sufficiently large (4.17 MJ/m^3 for 60% Co doping) to yield a high-performance permanent magnet.

To gain an insight into the stability of these alloys, we also compute the formation energy values (E^{for}) with respect to elemental decomposition, which are listed in Table I. We observe that all of the compounds studied



here have negative formation energy, indicating that all alloys are stable against elemental decomposition. Among the systems explored here, $\text{Ce}_2\text{ZrFe}_{15}$ shows the least formation energy of -44 meV/atom, whereas the formation energy of $\text{Ce}_2\text{ZrCo}_{15}$ is -112 meV/atom. Interestingly, with increasing x (Co concentration) in $\text{Ce}_2\text{ZrFe}_{15-x}\text{Co}_x$ and at $x = 9$ (at 60% Co doping), it becomes -110 meV/atom, which is comparable to that of $\text{Ce}_2\text{ZrCo}_{15}$. This finding of substantial negative formation energy on the Co-rich side of the alloy is a strong indication of the likely experimental feasibility of synthesis of these compounds.

One may make a projection of the potential-energy product BH_{max} of suitably optimized alloys in this family from these results. The $T = 0$ magnetization M_s of our $\text{Ce}_2\text{Fe}_6\text{Co}_9\text{Zr}$ alloy, at $27.15 \mu_B$ per formula unit, on a volumetric basis, is some 1.26 T. Given the calculated MAE constant K_1 of 7.78 MJ/m³, the magnetic hardness parameter $\kappa = K_1/\mu_0 M_s^2$ takes the value $\kappa = 6.19 \gg 1$, indicating that the maximum possible energy product $M_s^2/4$, or 40 MG Oe, should be achievable at low temperature. At the technologically relevant room temperature, with a slightly smaller moment this value would be closer to 32 MG Oe, assuming a 10% reduction in M_s at room temperature. While we make no detailed study of the Curie point of these alloys, previous work finds the Curie point of Zr-alloyed $\text{Ce}_2\text{Co}_{17}$ [10,12] to be of the order of 900 K, so that we anticipate only a small magnetization reduction due to temperature effects.

There is a compensating factor, however, that makes the 300 K achievable performance in this alloy system more likely the original 40 MG Oe figure. The κ value quoted above, deriving largely from the distortion of the 2-17 structure toward the 1-5 structure by Zr, is sufficiently large that smaller concentrations of Zr than the full substitution (approximately 7.5% by weight) modeled here

FIG. 6. (a) The configuration used to model 20, 40, 60, and 80% Co doping via the supercell method. (b) The total magnetic (spin plus orbital) moment and (c) the MAE calculated under GGA + SOC + U as a function of x in $\text{Ce}_2\text{ZrFe}_{15-x}\text{Co}_x$. The symbols correspond to the calculated compositions and the line is a guide to the eye. Results from VCA calculations (red filled squares) are also shown for comparison. The results from calculations without the Hubbard U are shown as green dotted lines with open diamonds.

may well produce optimal performance. This is, in fact, known from previous work on $\text{Sm}_2\text{Co}_{17}$ -based magnets, for which typical mass concentrations of magnets in actual usage are of the order of 3 wt% [54]. As noted above, Zr (due largely to its substituting for two $3d$ atoms) has a disproportionate effect on the magnetic moment and so one may envision an alloy composed of effectively equal proportions of our $\text{Ce}_2\text{Fe}_6\text{Co}_9\text{Zr}$ considered in detail here and $\text{Ce}_2(\text{Fe}_{0.4}\text{Co}_{0.6})_{17}$ as a means of simulating a lower Zr content. Since MAE is generally an atomic level quantity, we may consider that the MAE of such an alloy should be approximately the mean of these two quantities, which we find to be 3.6 MJ/m³, so that one still finds sufficient MAE for a strong permanent magnet. One may make a similar argument concerning the magnetization and, from direct calculation, we find the magnetization of $\text{Ce}_2(\text{Fe}_{0.4}\text{Co}_{0.6})_{17}$ to be some $32.5 \mu_B$ per formula unit, so that the magnetization of our lower-Zr alloy (averaging these two components) would be some 1.4 T at low temperature, or likely approximately 1.26 T or larger at room temperature. One would then recover the original potential-energy product of this alloy of 40 MG Oe but at room temperature. As with present SmCo-based magnets, the much higher likely Curie point than $\text{Nd}_2\text{Fe}_{14}\text{B}$ (585 K) means that above room temperature, these magnets would likely outperform Nd-based magnets by a substantial margin.

IV. CONCLUSIONS

By performing first-principles calculations, we carry out a detailed study of the magnetic properties of $\text{Ce}_2\text{Fe}_{17}$ and $\text{Ce}_2\text{Co}_{17}$ under Zr substitution at the dumbbell site. While we find that Zr doping has no favorable effect on the MAE of $\text{Ce}_2\text{Fe}_{17}$, consistent with previous reports, for $\text{Ce}_2\text{Co}_{17}$ we show that the MAE can be significantly improved by

one Zr substitution at the Co₂ dumbbell site. In order to further improve the magnetic properties, the total magnetization and MAE are calculated, at a few selected concentrations between Ce₂Fe₁₅Zr and Ce₂Co₁₅Zr within the VCA method. We show that the MAE can be significantly tuned by varying the Co concentration and that it switches from planar to uniaxial at 40% Co doping. The calculated MAE exhibits a strong dependence on the Co concentration and peaks at 60% Co doping (in Ce₂Fe₉Co₆Zr), which is more than twice as high as the MAE value calculated in the end-member compound Ce₂Co₁₅Zr. Very importantly, Ce₂Fe₉Co₆Zr still maintains a relatively high value of saturation magnetization (approximately 1.3 times higher than that of Ce₂Co₁₅Zr). These calculations suggest that the 60% Co Zr-alloyed material has potential room-temperature energy products as high as 40 MG Oe and likely a better temperature dependence than Nd₂Fe₁₄B. By analyzing the electronic DOS, we assess that the switching of the MAE from planar to uniaxial in Ce₂ZrFe_{15-x}Co_x, is likely related to Ce valence fluctuations in these compounds. This is further corroborated by the observed enhancement in the Ce spin and orbital magnetic moments. We hope that our current theoretical findings will stimulate experimental exploration of the magnetic properties of Zr- and Fe-alloyed Ce₂Co₁₇ alloys.

DATA AVAILABILITY

The Department of Energy will provide public access to these results of federally sponsored research in accordance with the DOE Public Access Plan [55].

ACKNOWLEDGMENTS

This research was supported by the Critical Materials Institute, an Energy Innovation Hub funded by the U.S. Department of Energy, Office of Energy Efficiency and Renewable Energy, Advanced Manufacturing Office. This research used resources of the Compute and Data Environment for Science (CADES) at the Oak Ridge National Laboratory, which is supported by the Office of Science of the U.S. Department of Energy under Contract No. DE-AC05-00OR22725. This manuscript has been authored by UT-Battelle, LLC under Contract No. DE-AC05-00OR22725 with the U.S. Department of Energy. The U.S. Government retains and the publisher, by accepting the article for publication, acknowledges that the U.S. Government retains a nonexclusive, paid-up, irrevocable, worldwide license to publish or reproduce the published form of this manuscript, or allow others to do so, for U.S. Government purposes.

[1] M. A. Susner, B. S. Conner, B. I. Saparov, M. A. McGuire, E. J. Crumlin, G. M. Veith, H. Cao, K. V. Shanavas, D. S.

- Parker, and B. C. Chakoumakos, *et al.*, Growth and characterization of Ce-substituted Nd₂Fe₁₄B single crystals, *J. Magn. Magn. Mater.* **434**, 1 (2017).
- [2] B. Conner, M. McGuire, K. Shanavas, D. Parker, and B. Sales, Evolution of structural and magnetic properties in La_xCe_{2-x}Co₁₆Ti for 0 ≤ x ≤ 2, *J. Alloys Compd.* **695**, 2266 (2017).
- [3] T. Pandey, M.-H. Du, and D.S. Parker, Tuning the Magnetic Properties and Structural Stabilities of the 2-17-3 Magnets Sm₂Fe₁₇X₃ (X = C, N) by Substituting La or Ce for Sm, *Phys. Rev. Appl.* **9**, 034002 (2018).
- [4] J. Jin, Y. Zhang, G. Bai, Z. Qian, C. Wu, T. Ma, B. Shen, and M. Yan, Manipulating Ce valence in RE₂Fe₁₄B tetragonal compounds by La-Ce co-doping: Resultant crystallographic and magnetic anomaly, *Sci. Rep.* **6**, 30194 (2016).
- [5] T. N. Lamichhane, V. Taufour, A. Palasyuk, Q. Lin, S. L. Budko, and P. C. Canfield, Ce_{3-x}Mg_xCo₉: Transformation of a Pauli Paramagnet into a Strong Permanent Magnet, *Phys. Rev. Appl.* **9**, 024023 (2018).
- [6] T. Pandey and D. S. Parker, Borderline Magnetism: How Adding Mg to Paramagnetic CeCo₃ Makes a 450-K Ferromagnet with Large Magnetic Anisotropy, *Phys. Rev. Appl.* **10**, 034038 (2018).
- [7] M. Bartashevich, T. Goto, R. Radwanski, and A. Korolyov, Magnetic anisotropy and high-field magnetization process of CeCo₅, *J. Magn. Magn. Mater.* **131**, 61 (1994).
- [8] T. N. Lamichhane, M. T. Onyszczak, O. Palasyuk, S. Sharikadze, T.-H. Kim, Q. Lin, M. J. Kramer, R. McCallum, A. L. Wysocki, M. C. Nguyen, *et al.*, Single-Crystal Permanent Magnets: Extraordinary Magnetic Behavior in the Ta-, Cu-, and Fe-Substituted CeCo₅ Systems, *Phys. Rev. Appl.* **11**, 014052 (2019).
- [9] R. Streever, Individual Co site contributions to the magnetic anisotropy of RCo₅ compounds and related structures, *Phys. Rev. B* **19**, 2704 (1979).
- [10] H. Fujii, M. Satyanarayana, and W. Wallace, Magnetic and crystallographic properties of substituted Ce₂Co_{17-x}T_x compounds (T = Ti, V, Cr, Mn, Fe, Cu, Zr, and Hf), *J. Appl. Phys.* **53**, 2371 (1982).
- [11] Z.-g. Sun, S.-y. Zhang, H.-w. Zhang, J.-y. Wang, and B.-g. Shen, The effect of manganese substitution on the magnetic properties of Ce₂Co₁₇ compounds, *J. Phys. Condens. Matter* **12**, 2495 (2000).
- [12] H. Fujii, M. Satyanarayana, and W. Wallace, Effect of substitution of Zr on the magnetic properties of R₂Co₁₇ (R = Ce and Sm), *Solid State Commun.* **41**, 445 (1982).
- [13] X. Wei, S. Hu, D. Zeng, X. Kou, Z. Liu, E. Brück, J. Klaasse, F. De Boer, and K. Buschow, Structure and magnetic properties of Ce₂Co_{17-x}Si_x compounds, *Phys. B: Condens. Matter* **262**, 306 (1999).
- [14] S. Hu, X. Wei, D. Zeng, X. Kou, Z. Liu, E. Brück, J. Klaasse, F. De Boer, and K. Buschow, Structure and magnetic properties of Ce₂Co_{17-x}Al_x compounds, *J. Alloys Compd.* **283**, 83 (1999).
- [15] B.-g. Shen, Z.-h. Cheng, S.-y. Zhang, J.-y. Wang, B. Liang, H.-w. Zhang, and W.-s. Zhan, Magnetic properties of R₂Co₁₅Al₂ compounds with R = Y, Ce, Pr, Nd, Sm, Gd, Tb, Dy, Ho, Er, and Tm, *J. Appl. Phys.* **85**, 2787 (1999).

- [16] P. Larson and I. Mazin, Effect of lattice relaxation on magnetic anisotropy: Zr-doped Sm_2Co_17 , *Phys. Rev. B* **69**, 012404 (2004).
- [17] L. Ke, D. Kukusta, and D. D. Johnson, Origin of magnetic anisotropy in doped Ce_2Co_17 alloys, *Phys. Rev. B* **94**, 144429 (2016).
- [18] D. Singh, *Planes Waves, Pseudopotentials, and the LAPW Method* (Kluwer Academic, Springer, Berlin, 1994).
- [19] E. Sjöstedt, L. Nordström, and D. Singh, An alternative way of linearizing the augmented plane-wave method, *Solid State Commun.* **114**, 15 (2000).
- [20] P. Blaha, K. Schwarz, G. K. H. Madsen, D. Kvasnicka, and J. Luitz, WIEN2K, *An Augmented Plane Wave + Local Orbitals Program for Calculating Crystal Properties* (Karlheinz Schwarz, Technische Universität Wien, Austria, 2001).
- [21] L. Vegard, Die Konstitution der Mischkristalle und die Raumbildung der Atome, *Z. Phys.* **5**, 17 (1921).
- [22] A. R. Denton and N. W. Ashcroft, Vegard's law, *Phys. Rev. A* **43**, 3161 (1991).
- [23] J. P. Perdew, K. Burke, and M. Ernzerhof, Generalized Gradient Approximation Made Simple, *Phys. Rev. Lett.* **77**, 3865 (1996).
- [24] D. D. Koelling and B. N. Harmon, A technique for relativistic spin-polarised calculations, *J. Phys. C: Solid State Phys.* **10**, 3107 (1977).
- [25] H. Lu and L. Huang, Pressure-driven $4f$ localized-itinerant crossover in heavy-fermion compound CeIn_3 : A first-principles many-body perspective, *Phys. Rev. B* **94**, 075132 (2016).
- [26] H. Lu and L. Huang, Itinerant-localized crossover and orbital dependent correlations for $4f$ electrons in cerium-based ternary 122 compounds, *Phys. Rev. B* **98**, 195102 (2018).
- [27] W. Temmerman, L. Petit, A. Svane, Z. Szotek, M. Lüders, P. Strange, J. Staunton, I. Hughes, and B. L. Gyorffy, *Handbook on the Physics and Chemistry of Rare Earths* (Elsevier Science, Amsterdam, The Netherlands, 2009), Vol. 39, p. 1.
- [28] V. I. Anisimov, J. Zaanen, and O. K. Andersen, Band theory and Mott insulators: Hubbard U instead of Stoner I , *Phys. Rev. B* **44**, 943 (1991).
- [29] A. Svane, Electronic Structure of Cerium in the Self-Interaction Corrected Local Spin Density Approximation, *Phys. Rev. Lett.* **72**, 1248 (1994).
- [30] A. Svane, W. Temmerman, and Z. Szotek, Theory of pressure-induced phase transitions in cerium chalcogenides, *Phys. Rev. B* **59**, 7888 (1999).
- [31] V. I. Anisimov, I. Solovyev, M. Korotin, M. Czyżyk, and G. Sawatzky, Density-functional theory and NiO photoemission spectra, *Phys. Rev. B* **48**, 16929 (1993).
- [32] A. Liechtenstein, V. Anisimov, and J. Zaanen, Density-functional theory and strong interactions: Orbital ordering in Mott-Hubbard insulators, *Phys. Rev. B* **52**, R5467 (1995).
- [33] I. Solovyev, P. Dederichs, and V. Anisimov, Corrected atomic limit in the local-density approximation and the electronic structure of d impurities in Rb, *Phys. Rev. B* **50**, 16861 (1994).
- [34] D. Givord and R. Lemaire, Magnetic transition and anomalous thermal expansion in R_2Fe_17 compounds, *IEEE Trans. Magn.* **10**, 109 (1974).
- [35] D. Middleton and K. Buschow, Magnetic properties of $\text{Ce}_2\text{Fe}_{17-x}\text{Si}_x$ compounds, *J. Alloys Compd.* **206**, L1 (1994).
- [36] S. R. Mishra, G. J. Long, O. A. Pringle, D. Middleton, Z. Hu, W. B. Yelon, F. Grandjean, and K. Buschow, A magnetic, neutron diffraction, and Mössbauer spectral study of the $\text{Ce}_2\text{Fe}_{17-x}\text{Al}_x$ solid solutions, *J. Appl. Phys.* **79**, 3145 (1996).
- [37] Y. Janssen, S. Chang, A. Kreyssig, A. Kracher, Y. Mozharivskyj, S. Misra, and P. Canfield, Magnetic phase diagram of Ce_2Fe_17 , *Phys. Rev. B* **76**, 054420 (2007).
- [38] A. Teplykh, A. Pirogov, and A. Kuchin, Magnetic structure of $\text{Ce}_2\text{Fe}_{17-x}\text{Mn}_x$ intermetallic compounds, *Phys. Solid State* **52**, 922 (2010).
- [39] See the Supplemental Material at <http://link.aps.org-supplemental/10.1103/PhysRevApplied.13.034039> for energetics of various magnetic configurations of $\text{Ce}_2\text{ZrFe}_{15-x}\text{Co}_x$ alloys, and effect of Hubbard U on magnetic anisotropy energy, and density of states..
- [40] X. Xu and S. A. Shaheen, Structural and magnetic properties of rare earth iron nitride series $\text{R}_2(\text{Fe}_{1-x}\text{Co}_x)_{17}\text{N}_{3-\delta}$, *J. Appl. Phys.* **73**, 1892 (1993).
- [41] R. K. Chouhan and D. Paudyal, Cu substituted CeCo_5 : New optimal permanent magnetic material with reduced criticality, *J. Alloys Compd.* **723**, 208 (2017).
- [42] O. Isnard, S. Miraglia, D. Fruchart, C. Giorgetti, E. Dartige, and G. Krill, X-ray absorption spectroscopy and magnetic circular x-ray dichroism in $\text{Ce}_2\text{Fe}_17\text{N}_3$, *J. Phys. Condens. Matter* **8**, 2437 (1996).
- [43] O. Isnard, S. Miraglia, C. Giorgetti, E. Dartige, G. Krill, and D. Fruchart, Ce valence state probed by XAFS study in $\text{Ce}_2\text{Fe}_{17-x}\text{Ga}_x\text{H}_y$ compounds, *J. Alloys Compd.* **262**, 198 (1997).
- [44] J. Coey, J. Allan, A. Minakov, and Y. V. Bugaslawsky, $\text{Ce}_2\text{Fe}_{17}$: Mixed valence or $4f$ band? *J. Appl. Phys.* **73**, 5430 (1993).
- [45] R. Neifeld, M. Croft, T. Mihalisin, C. Segre, M. Madigan, M. Torikachvili, M. Maple, and L. DeLong, Chemical environment and Ce valence: Global trends in transition-metal compounds, *Phys. Rev. B* **32**, 6928 (1985).
- [46] B. C. Sales, A model for the thermodynamic properties of metallic rare earth systems with an unstable valence, *J. Low Temp. Phys.* **28**, 107 (1977).
- [47] B. Sales and D. Wohlleben, Susceptibility of interconfiguration-fluctuation compounds, *Phys. Rev. Lett.* **35**, 1240 (1975).
- [48] A. Alam and D. D. Johnson, Mixed valency and site-preference chemistry for cerium and its compounds: A predictive density-functional theory study, *Phys. Rev. B* **89**, 235126 (2014).
- [49] P. Bruno, Tight-binding approach to the orbital magnetic moment and magnetocrystalline anisotropy of transition-metal monolayers, *Phys. Rev. B* **39**, 865 (1989).
- [50] L. Steinbeck, M. Richter, and H. Eschrig, Magnetocrystalline anisotropy of RCo_5 intermetallics: Itinerant-electron contribution, *J. Magn. Magn. Mater.* **226**, 1011 (2001).
- [51] A. Edström, M. Werwiński, D. Iușan, J. Rusz, O. Eriksson, K. Skokov, I. Radulov, S. Ener, M. Kuzmin, J. Hong, et al., Magnetic properties of $(\text{Fe}_{1-x}\text{Co}_x)_2\text{B}$ alloys and the

- effect of doping by 5d elements, *Phys. Rev. B* **92**, 174413 (2015).
- [52] S. Steiner, S. Khmelevskyi, M. Marsmann, and G. Kresse, Calculation of the magnetic anisotropy with projected-augmented-wave methodology and the case study of disordered $\text{Fe}_{1-x}\text{Co}_x$ alloys, *Phys. Rev. B* **93**, 224425 (2016).
- [53] M. Däne, S. K. Kim, M. P. Surh, D. Åberg, and L. X. Benedict, Density functional theory calculations of magnetocrystalline anisotropy energies for $(\text{Fe}_{1-x}\text{Co}_x)_2\text{B}$, *J. Phys. Condens. Matter* **27**, 266002 (2015).
- [54] J. Ormerod, Personal communication.
- [55] <https://www.energy.gov/downloads/doe-public-access-plan>.